HHS Public Access

Author manuscript

Chemosens Percept. Author manuscript; available in PMC 2023 October 13.

Published in final edited form as:

Chemosens Percept. 2022 October ; 15(2): 124–134. doi:10.1007/s12078-022-09300-2.

A Nasal Aerodynamics Perspective of Retronasal Olfaction: Rodents vs. Humans

Kanghyun Kim[1,2], **Kai Zhao**[1,2]

[1]Department of Otolaryngology - Head & Neck Surgery, The Ohio State University, Columbus, OH

[2]Department of Biomedical Engineering, The Ohio State University, Columbus, OH

Abstract

Introduction: Odor perception can be achieved through ortho or retronasal routes, with the latter being an important component of flavor perception. There are significant olfactory differences that exist between rats and humans and by understanding the role of structural differences, further insight can be gained into the mechanism of odorant perception via ortho or retronasal routes.

Methods: 3D human and rat (Sprague Dawley) computational models were used to investigate nasal anatomy impact on ortho vs. retronasal odorant transport to the olfactory epithelium. The nasal pharynx region was modified for human and rat models to probe nasal structure impact on ortho vs retro olfaction. 65 odorant absorption rates to the olfactory epithelium were extracted from each model.

Results: For human, the retronasal route provided higher peak odorant absorption compared to orthonasal route (left: 90% higher, right: 45% higher), but substantially lowered peak absorption for rat (medial: 97% lower, lateral: 75% lower). For both models, anatomical modification had minimal impact to orthonasal routes, but substantially modulated the retronasal route: decrease (left: −41.4%, right: −44.2%) for human, and increase to the medial (29.5%) but not to lateral (−14.3%) for rat.

Conclusions: There exist key differences between humans and rats regarding retro/orthonasal odorant transport routes, which matched well with experimental olfactory bulb activity data in literature.

Implications: While humans have equivalent odorant delivery between routes, the difference in retro and orthonasal routes in rodents is substantial and changes to the transverse lamina above the nasopharynx can substantially modulate the retronasal route, but not enough to bridge the gap between the two routes.

Corresponding Author: Kai Zhao, PhD, Associate Professor, Department of Otolaryngology - Head & Neck Surgery, The Ohio State University, 915 Olentangy River Rd., Office 4235, Columbus, OH 43212, 614-293-3857 (office); 614-366-1794 (lab); 614-293-7476 (fax), zhao.1949@osu.edu;.

Competing Interests: The authors have no relevant financial or non-financial interests to disclose.

Ethics Approval: Approval for the procedures in this study was gained from the Ohio State University Institutional Review Board.

Consent: Informed consent was obtained from all individual participants included in the study.

Keywords

CFD; Simulation; Odorant Distribution; Airflow; Steady-State; Rodent

Introduction

Odorant access to the olfactory epithelium can be achieved through two routes: orthonasal, where odorants enter the nasal cavity through inhalation/sniffing via the nostrils; and retronasal, where odorants released from food in the mouth enter the nasal cavity through exhalation via the nasopharynx. There has been extensive investigation into the role of different routes of olfaction in the differences in perception of odorants. Recent work by Hannum et al. (2018) as well as Heilmann and Hummel (2006) report that there is a perceptual difference for odorants between the retro and orthonasal route[1,2]. Work by Pierce and Simons (2018) also observed that odorants differed in the level of adaptation when it came to retro and orthonasal smelling[3]. Differences in retro and orthonasal olfaction have also been highlighted when looking at diseased patients. Clinically, Cowart, et al (1999, 2003) reported that defects in retronasal smelling can occur in the absence of orthonasal deficits[4,5]. On the other hand, better retro than orthonasal olfactory function among patients with chronic rhinosinusitis (CR) and nasal polyposis (NP) was observed by Landis et al. (2003, 2005)[6,7]. In order to explain the difference in odorant perception, Rozin (1982) considered these routes as two distinct systems and hypothesized that the perception depends on the odor route[8]. Experimental studies by Heilmann and Hummel (2004) and Sun and Halpern (2005) along with additional human brain imaging studies by Small et al. (2005) seem to support this hypothesis and suggest that ortho and retronasal delivery of the same odorant will invoke distinct neurological responses to the cortical areas of the brain, leading to differing perceptions of the same odorant[9–11]. Computational studies by Zhao et al. (2006) have shown that there are airflow differences when it comes to ortho and retronasal breathing, which could also serve as another explanation for these discrepancies in perception[12].

In addition to experimental work in humans, significant efforts have been made to understand olfactory function using rodents as a model system. Similar to humans, there has been behavioral and direct neurological evidence in rats and mice that show significant differences between retronasal vs orthonasal olfaction, especially in response magnitude[13–15]. However, there are significant differences in nasal cavity anatomy between humans and rats, which could result in considerable differences in flow patterns and odorant transport to the olfactory epithelium during retro and orthonasal routes. For humans, there is little physical separation when it comes to airflow access from the main nasal airway to the olfactory epithelium, during either orthonasal or retronasal breathing. In comparison, rodents' olfactory epithelium is physically bounded and confined in the posterior region of the nasal cavity. The olfactory recess is separated from the ventral nasopharynx by a transverse lamina (Figure 1c), a quite common structure in many mammals[29]. This sequestered region allows for air to travel into the olfactory recess during orthonasal transport but may limit airflow during retronasal transport. Also, the olfactory epithelium for humans is a structurally simple cleft. In contrast, rodents possess a much more complex

and intricate olfactory epithelium with multiple folds. There have been studies that have observed that olfactory odorant transport can be differentially altered by modifying key regional nasal structures[19–21]. Further research to quantify these differences is important to potentially translate findings from rodent models to humans.

On the other hand, the 'chromatographic' theory of the olfactory system (Mozell, 1970), which hypothesized that odor flow parameters can lead to differential odorant distribution across the olfactory epithelium (Scott-Johnson et al., 2000), can further exacerbate the difference between retro and orthonasal route in humans vs rodents[16,17]. Odorant transport simulations utilizing computational fluid dynamics (CFD) models have been done previously with Keyhani et al. (1997) and later with studies from Zhao et al. (2004)[18,19]. However, such odorant distribution models have yet to be used to investigate the differences in odorant absorption between rodents and humans with regards to the ortho vs retronasal route. Thus, the first goal of this study is to utilize a modeling approach to examine any fundamental differences or similarities in ortho and retronasal olfaction between rodents and humans. The second goal is to evaluate whether a modification of nasal structure would impact olfactory odorant uptake, as an attempt to further probe the relationship between nasal structure and olfactory airflow. Through these goals, more insight can be obtained into why such differences exist between the two routes and between difference species and the role that nasal cavity structure can play.

Methodology

Anatomically Accurate Computational models

Human: A previously published 3-D anatomically accurate computational nasal cavity model (Zhao et al., 2004) created based on Computerized Tomography (CT) images of a healthy human female was used for this study[19]. In brief, the model was built by creating a clear boundary between the nasal mucosa and the surrounding air through tracing the nasal airway for each CT slice using specialized software (AMIRA®, Thermo Fisher Scientific, Waltham, MA). A 3-D geometric model was then created by stacking and combining the multiple slices together. A tetrahedral element mesh was then generated to fill the nasal cavity air space using grid generation software (ICEM CFD®, Ansys Inc, Canonsburg, PA). A finer mesh was created near the mucosal surface to accurately model the rapidly changing air velocity and odorant concentration in that region (Zhao et al., 2004)[19]. In total the surface mesh had 449,079 elements and the nasal cavity interior was populated with 7,094,099 elements. The olfactory epithelium was identified and marked on the appropriate air/mucosal interface location according to anatomical and functional studies[22,23]. This can be seen in Figure 2a and 2b.

Rat: A published computational model of the rat nasal passage was used in this study[28]. It was developed from the CT scan of a Sprague-Dawley rat nasal cavity using similar geometry and mesh generation methods. Grid-independence was confirmed by doubling the grid number, which showed negligible effects on the simulation results, i.e., the flow field and particle concentration field are stable. In total, the surface mesh of the rat model

had 1,044,121 elements and the interior of the nasal cavity was populated with 6,382,827 elements. The model of the rodent nasal cavity is shown in Figure 1a and 1b.

Anatomical Modification

Since there is much difference in the nasal anatomies between the two species, we propose to modify certain key structures to investigate their impact to ortho vs retronasal odorant transport. In a previous study by Leopold (1988), three nasal regions were identified to be critical and likely to impact olfactory functions[24]. Due to the interest in retronasal airflow, for the human model, the cleft region which is directly posterior to the olfactory epithelium and superior to the nasal pharynx was chosen as the region of interest, as it may potentially restrict airflow from the nasopharynx to the olfactory cleft. According to the method described by Zhao et al. (2004), the region posterior to the olfactory cleft was obstructed by reducing the volume of that section by 62.74%[19]. Figure 2c shows the overlay of the coronal cross sections of the original and narrowed nasal airway models with the corresponding CT images.

To expand access of the olfactory region for the rat model, the transverse lamina that sequesters the olfactory recess ventrally from the nasopharynx for the rat was artificially removed as shown in Figure 1c, which is highlighted in green, and would hypothetically open the olfactory epithelium to more retronasal airflow and odorant access.

Airflow and Odorant Transport Simulations

Inspiratory and expiratory steady state laminar airflow was simulated with a commercial finite volume software (Fluent®, Ansys Inc, Canonsburg, PA) based on previously published methods[19]. In brief, for the human model, air was mathematically drawn into or out of the nostrils by an imposed pressure drop of 15 Pascal between the nostrils and the nasal pharynx for inspiration and the inlet and outlet was reversed for expiration. The selected magnitude of pressure drop resulted in bilateral nasal airflow rates of 240 ml/s to represent resting breathing rates, when the nasal airflow is mostly laminar (Hahn 1993, Keyhani, 1995)[25,26]. The magnitude of the pressure drop for the rat model was set to be 185.84 Pascal between the nostrils and nasal pharynx and reversed accordingly for retronasal flow, with resulting bilateral flowrate 8.5 ml/s representing restful breathing[12].

The steady state ortho and retronasal transport and mucosal uptake of vaporized odorants through airflow was then simulated using the estimated physio-chemical properties in both air phase and in mucosa[19,27,28]. Absorption of 65 different odorants with varying degree of mucosal solubility were modeled. Air/mucus partition coefficient was used to characterize solubility, with a lower partition coefficient indicating higher solubility in mucus. The odorant transport and absorption equation are linearly scaled to the incoming odorant air concentration when it is low (<5%v/v). In other words, if the air phase odorant concentration increased from 100 to 200 ppm, the absorption everywhere would double. Therefore, we used a standard arbitrary ambient concentration (100 ppm) for every odor. For humans, due to the olfactory epithelium being rather small (5.18% of total nasal surface area), the olfactory epithelium was averaged as one region. In contrast, the rat olfactory epithelium is large, thus we factor in a regional difference, and sampled two regions on the medial and

lateral part of the olfactory zone, as previously defined (see Figure 1a and 1b)[28]. Changes in nasal airflow and the amount of odorant that was absorbed into the targeted region during inhalation and exhalation were examined between the original and altered nasal cavity.

Data Analysis

CFD and odorant uptake data from the simulation was post processed to generate airflow streamlines as well as airflow velocity and odorant flux contour maps. With regards to odorant uptake data, CFD software (Fluent©) in conjunction with in-house built code was used to calculate and average the odorant flux data for the area of interest. Calculations and compiling of odorant uptake data were performed using a combination of spreadsheet (Excel®, Microsoft, Redmond, WA) and numeric computing software (MATLAB®, Mathworks, Natick, MA).

Results

Airflow Analysis (Rat vs Human)

Figure 3 shows the airflow velocity streamlines across the human nasal cavity. There is a region of high velocity air (red) passing through the middle and inferior meatus. Only a small percentage of mostly low velocity (green) streamlines pass through the olfactory epithelial region. This airflow pattern is consistent for both the ortho and retronasal route. The modification to the posterior region to the olfactory cleft had more impact on the distribution and velocities of the streamlines retronasally than orthonasally. We further examined the velocity profiles at two coronal cross sections that cut across the anterior and posterior olfactory epithelial region. Comparing Figure 3a and Figure 3b, modification to the airway has decreased the amount of high velocity air in the posterior section of the olfactory zone and is much more pronounced for retronasal than orthonasal airflow (see Figure 3c and 3d), which may indicate that airway modification will impact retronasal transport greater than orthonasal transport.

For rodent airflow, different flow profiles can be seen when compared to the human model. Looking at Figure 4a through Figure 4d, most of the high velocity airflow (red and yellow) travels along the main airway with limited streamlines entering the olfactory recess (lower velocity: blue and green). The panels to the right in Figure 4 show the cross-sectional views of the velocity contour, which exhibit little difference pre vs post modification either ortho or retronasally, except for the posterior slice around the olfactory region that is immediately superior to the removed transverse lamina (shown in Figure 4 as a boxed in region), where air streamline perturbation was observed following modification both ortho and retronasally.

Impact of Nasal Structure on Ortho vs Retronasal Olfactory Odor Absorption

Absorbed concentrations for 65 different odorants (see supplementary material) at the respective olfactory regions were plotted against their mucosal solubilities for both human and rat models (see Figure 5).

For human, modification to the posterior region to the olfactory cleft substantially decreased peak retronasal odorant absorption for both sides (left side: 41.4% decrease, right side:

44.2% decrease) while having a minimal effect on orthonasal odorant absorption (left side: 0.6% higher, right side: 9.5% lower). The absorption curves peak for intermediate solubility odorants, more prominently for orthonasal than retronasal, and then drop off for both extremes of the solubility spectrum, with low solubility odorants having the lowest absorption values (see Figure 5a and 5b).

The mucosal odor absorption pattern for the peak odorant (pyrazine) was plotted in Figure 6. It shows that there is very little change in odorant distribution pre- and post-modification for orthonasal transport, with both distributions showing most of the odorant concentration being absorbed around the anterior nasal cavity (See Figure 6a and 6b). For retronasal transport, a clear reduction of odorant flux in the posterior/inferior region of the olfactory zone can be seen after the modification (see Figure 6c and 6d).

Similar trend was observed in the rodent model, with some interesting exceptions. Looking at Figure 5d, there is only slight decrease in peak odorant flux after removal of the transverse lamina for both medial and lateral sample sites of the olfactory recess for orthonasal transport (medial: 3.4% decrease, lateral: 8.7% decrease). But for retronasal transport (see Figure 5c), the removal substantially increased odorant flux magnitude for the medial site (medial: 29.5% higher), but not for the lateral site (lateral: 14.3% decrease). The mucosal odor absorption map of the peak odorant (toluene) was plotted in Figure 7.

These maps confirmed the minor changes in odorant distribution between pre- and post-modification for orthonasal transport (See Figure 7a and 7b). For retronasal transport, the medial site showed a clear increase in odorant flux, indicating increased absorption of odorant (see Figure 7c and 7d). For both modes of transport, a local increase in odorant flux near the nasopharynx area was observed, which is consistent with the airflow analysis.

Simulation Validation

The simulation results from the CFD analysis of unmodified models were compared to experimental rat glomerular bulb response mapping from literature[13,28]. In the referenced study, Gautam and Verhagen reported the ratio of glomerular activity in the dorsal olfactory bulb when 6 odorants of different solubility were presented to the rodent through retro vs orthonasal routes. A ratio was calculated between retronasal and orthonasal odor absorption (R/O ratio) based on the CFD simulation results for the same odorants at the medial region, where the dorsal olfactory bulb activity corresponds to. The reported (R/O) ratios of the measured glomelular bulb response were found to be significantly correlated to the CFD R/O absorption ratios which are shown in Figure 8 (r=.941, P=.017), validating the model.

Discussion

The main results from this exploratory study showed that while modifications certainly altered odorant transport for both the rodent (especially the medial region) and human models, the changes were overall limited, especially for the orthonasal route. For the retronasal route, we see larger changes with a peak odor absorption increase of 29.5% at the medial site and decrease of 14.3% at the lateral site for rodent (see Figure 5), while the peak absorption decreased (left: 41.4%, right: 44.2%) for human. The modification of

nasal anatomy successfully targeted the retronasal route specifically for both species as hypothesized and the effect is not enough to overcome the intrinsic differences between the two routes, especially for the rat model, where the retronasal route produced substantially lower odorant delivery than the orthonasal route (peak R/O ratio medial: 3%, lateral: 25%). Even after modification the retro vs ortho-nasal ratio remains substantial (R/O medial: 4%, lateral: 24%). Conversely for the human model, the retronasal route provided a higher odorant delivery compared to the orthonasal route (peak R/O ratio left: 191%, right: 145%), where even after modification to limit the retronasal transport, the retro vs ortho-nasal ratio remains similar (R/O left: 111%, right: 89%).

Interestingly, there are clear asymmetries in nasal structure between the left and right side of the nasal cavity for both human and rat models (see cross sections in Figures 3 and 4), which are reflected in large deviations in the peak odorant uptake between left and right sides for both models. Clearly, such asymmetries substantially impact the airflow through the nasal cavity, resulting in asymmetric odorant uptake rate. The impact of nasal structure asymmetry has also been reported in other numerical simulation studies, where structural obstruction and volume differences between the two passages and different areas of the nasal cavity resulted in varying airflow velocity, which lead to varying profiles of odorant uptake[19,24].

Another observation is the difference in the odorant solubility for the peak absorption (See Figure 5) between human and rodent as well as between the two routes. For human, the peak occurred in higher solubility for the retronasal route (peak at 5.537e-05 air/mucus partition coefficient) than the ortho route (peak at 1.588e-04, smaller partition coefficient indicates higher solubility), which is consistent with literature[19]. Peak absorption is a tradeoff between an odorant's mucosal solubility and upstream absorption. If an odorant has low solubility, then of course the absorption would be low. But if an odorant has too high solubility, then much of the air concentration will be absorbed prior to the airflow reaching the olfactory region. So, the optimal peak uptake is often a balance between solubility and upstream absorption. Orthonasally, the longer distance from the nares to the olfactory epithelium (measured 6.4 cm vs 5.3 cm retronasally) in the human model means more of the high solubility odorants get absorbed earlier prior to reaching the olfactory region, leading to the peak or optimal uptake to occur for medium solubility odorants. Retronasally, with closer proximity from the nasopharynx to the olfactory epithelium, the optimal or peak uptake would occur for higher solubility odorants. This difference may hypothetically contribute to the reported difference in orthonasal and retronasal perception, which still needs to be investigated. On the other hand, for rodents, the peaks lean towards medium to low solubility odorants (retro: lateral peak at 4.9e-2 and medial peak at 4.9e-2, ortho: lateral peak at 8e-3 and medial peak at 2e-3), with the retro route leaning more towards the low solubility, which again can be attributed to the flow path differences and agrees with the report by Scott et al. (2014)[28]. The olfactory epithelium of the rodent is more restrictive to odorant access, as it is largely a one-way air trap, with the entrance into this recess favoring airflow going in the orthonasal direction. In contrast, due to this structural design, retronasal airflow is required to circulate back up into the olfactory recess opening, resulting a longer flow path.

With the modification, the human model showed a very small peak shift towards lower solubilities for both ortho and retronasal routes (<0.012%). In contrast, for the rodent model, only the medial site for retronasal airflow showed a moderate peak shift towards higher solubility odorants (2.31%) due to the more accessible flow path after modification. By creating an opening to the olfactory recess with the removal of transverse lamina, the improved airflow access can allow for higher solubility odorants to enter the olfactory recess without the need to traverse the nasal cavity, and this could explain the slight shift in odorant uptake curves towards higher solubility odorants for the medial site in retronasal flow. However, from the velocity profiles, most of the airflow still bypassed lateral olfactory recess, even after the modification. This may explain why the lateral site did not see any peak shifts during the retronasal route as the lateral site is more sequestered than the medial site, similar to what is observed in other mammalian species with transverse lamina structures[20,21].

We compared the CFD data against experimental rat glomerular bulb response mapping for the same odorants in literature and observed a significant positive correlation (r=.941, P=.017) shown in Figure 8[13,28]. The retro/ortho ratio between bulb response and CFD fit an exponential equation, which matches a typical stimulus to neural response exponential relationship, but with a very small exponent (0.0264) – a rather flat slope (Figure 8). For example, vinyl cyclohexane, which is a low soluble odorant, has a CFD R/O ratio of 0.465 and a bulb response R/O ratio of 0.62. On the other hand, O-tolualdehyde, which is a high soluble odorant, the CFD R/O ratio drops 11 orders of magnitude to 1.051e-11, which corresponds to only a 1.8 times reduction in R/O ratio of bulb response to 0.34. But the trend is consistent that odorants with lower mucosal solubility have a higher R/O ratio (closer to 1) in both CFD simulated absorption and bulb neural actvitities, and odorants with higher mucosal solubility have substantially reduced R/O ratios. But the reduction of bulb retronasal response is much more subdued, which may reflect substantial signal amplifications from the stimuli (mucosal odorant absorption) to the olfactory bulb response that bridges the differences. This could indicate that there are additional neural processes that contribute importantly to the final perceptual difference between ortho vs retronasal responses.

Limitations

Limitations of this exploratory study include: one model each for the human and rodent was evaluated. Therefore, individual variability when it comes to odorant uptake and nasal cavity airflow is possible. As a quasi-steady simulation, this study does not capture the sniffing behavior that rodents exhibit in the normal odorant sampling behavior. Further investigation into the impact of the modification with full sniffing cycle could provide further insight. Nevertheless, this study illuminates the significant discrepancy between rodent and human anatomy and their differential impacts on ortho vs retro olfactory functions.

Conclusion

In summary, there exist clear differences in human and rat odorant uptake behavior, and significant species' difference between retro and orthonasal odor transport routes. While

humans have equivalent odorant delivery between routes, the difference in retro and orthonasal routes in rodents is substantial and changes to the transverse lamina above the nasopharynx can differentially modulate the retronasal route, but not enough to bridge the gap between the two routes.

Supplementary Material

Refer to Web version on PubMed Central for supplementary material.

Funding:

This research was supported by NIH NIDCD R01 DC013626 and R21 DC017530 to Kai Zhao.

References

1. Hannum M, Stegman MA, Fryer JA, Simons CT. Different Olfactory Percepts Evoked by Orthonasal and Retronasal Odorant Delivery. Chemical Senses. 2018;43(7):515–521. doi:10.1093/chemse/bjy043 [PubMed: 29982522]
2. Hummel T, Heilmann S, Landis BN, et al. Perceptual differences between chemical stimuli presented through the ortho- or retronasal route. Flavour and Fragrance Journal. 2006;21(1):42–47. doi:10.1002/ffj.1700
3. Pierce AM, Simons CT. Olfactory Adaptation is Dependent on Route of Delivery. Chemical Senses. 2018;43(3):197–203. doi:10.1093/chemse/bjy007 [PubMed: 29401258]
4. Cowart BJ, Halpern BP, Varga EK. A Clinical Test of Retronasal Olfaction. Chemical Senses. 1999;24(608).
5. Cowart BJ, Halpern BP, Rosen D, Klock CT, Pribitkin EA. Differential Loss of Retronasal Relative to Orthonasal Olfaction in a Clinical Population. Chemical Senses. 2003;24(A65).
6. Landis BN, Giger R, Ricchetti A, et al. Retronasal olfactory function in nasal polyposis. The Laryngoscope. 2003;113(11):1993–1997. doi:10.1097/00005537-200311000-00026 [PubMed: 14603062]
7. Landis BN, Frasnelli J, Reden J, Lacroix JS, Hummel T. Differences Between Orthonasal and Retronasal Olfactory Functions in Patients With Loss of the Sense of Smell. Archives of Otolaryngology–Head & Neck Surgery. 2005;131(11):977. doi:10.1001/archotol.131.11.977 [PubMed: 16301369]
8. Rozin P “Taste-smell confusions” and the duality of the olfactory sense. Perception & Psychophysics. 1982;31(4):397–401. doi:10.3758/BF03202667 [PubMed: 7110896]
9. Heilmann S, Hummel T. A New Method for Comparing Orthonasal and Retronasal Olfaction. Behavioral Neuroscience. 2004;118(2):412–419. doi:10.1037/0735-7044.118.2.412 [PubMed: 15113268]
10. Sun BC, Halpern BP. Identification of Air Phase Retronasal and Orthonasal Odorant Pairs. Chemical Senses. 2005;30(8):693–706. doi:10.1093/chemse/bji062 [PubMed: 16177226]
11. Small DM, Gerber JC, Mak YE, Hummel T. Differential Neural Responses Evoked by Orthonasal versus Retronasal Odorant Perception in Humans. Neuron. 2005;47(4):593–605. doi:10.1016/j.neuron.2005.07.022 [PubMed: 16102541]
12. Zhao K, Pribitkin EA, Cowart BJ, Rosen D, Scherer PW, Dalton P. Numerical Modeling of Nasal Obstruction and Endoscopic Surgical Intervention: Outcome to Airflow and Olfaction. American Journal of Rhinology. 2006;20(3):308–316. doi:10.2500/ajr.2006.20.2848 [PubMed: 16871935]
13. Gautam SH, Verhagen JV. Retronasal Odor Representations in the Dorsal Olfactory Bulb of Rats. Journal of Neuroscience. 2012;32(23):7949–7959. doi:10.1523/JNEUROSCI.1413-12.2012 [PubMed: 22674270]
14. Gautam SH, Verhagen JV. Direct Behavioral Evidence for Retronasal Olfaction in Rats. Schaefer A, ed. PLoS ONE. 2012;7(9):e44781. doi:10.1371/journal.pone.0044781 [PubMed: 22970305]

15. Rebello MR, Kandukuru P, Verhagen JV. Direct Behavioral and Neurophysiological Evidence for Retronasal Olfaction in Mice. Hummel T, ed. PLOS ONE. 2015;10(2):e0117218. doi:10.1371/journal.pone.0117218 [PubMed: 25675095]

16. Mozell MM. Evidence for a Chromatographic Model of Olfaction. The Journal of General Physiology. 1970;56(1):46–63. doi:10.1085/jgp.56.1.46 [PubMed: 5514160]

17. Scott-Johnson PE. Effects of Air Flow on Rat Electroolfactogram. Chemical Senses. 2000;25(6):761–768. doi:10.1093/chemse/25.6.761 [PubMed: 11114154]

18. Keyhani K, Scherer PW, Mozell MM. A Numerical Model of Nasal Odorant Transport for the Analysis of Human Olfaction. Journal of Theoretical Biology. 1997;186(3):279–301. doi:10.1006/jtbi.1996.0347 [PubMed: 9219668]

19. Zhao K Effect of Anatomy on Human Nasal Air Flow and Odorant Transport Patterns: Implications for Olfaction. Chemical Senses. 2004;29(5):365–379. doi:10.1093/chemse/bjh033 [PubMed: 15201204]

20. Eiting TP, Perot JB, Dumont ER. How much does nasal cavity morphology matter? Patterns and rates of olfactory airflow in phyllostomid bats. Proceedings of the Royal Society B: Biological Sciences. 2014;282(1800):20142161–20142161. doi:10.1098/rspb.2014.2161

21. Eiting TP, Smith TD, Perot JB, Dumont ER. The role of the olfactory recess in olfactory airflow. Journal of Experimental Biology. 2014;217(10):1799–1803. doi:10.1242/jeb.097402 [PubMed: 24577441]

22. Féron F, Perry C, McGrath JJ, Mackay-Sim A. New Techniques for Biopsy and Culture of Human Olfactory Epithelial Neurons. Archives of Otolaryngology–Head & Neck Surgery. 1998;124(8):861. doi:10.1001/archotol.124.8.861 [PubMed: 9708710]

23. Restrepo D, Okada Y, Teeter JH, Lowry LD, Cowart B, Brand JG. Human olfactory neurons respond to odor stimuli with an increase in cytoplasmic Ca2+. Biophysical Journal. 1993;64(6):1961–1966. doi:10.1016/S0006-3495(93)81565-0 [PubMed: 8369416]

24. Leopold DA. The Relationship Between Nasal Anatomy and Human Olfaction. The Laryngoscope. 1988;98(11):1232–1238. doi:10.1288/00005537-198811000-00015 [PubMed: 3185078]

25. Hahn I, Scherer PW, Mozell MM. Velocity profiles measured for airflow through a large-scale model of the human nasal cavity. Journal of Applied Physiology. 1993;75(5):2273–2287. doi:10.1152/jappl.1993.75.5.2273 [PubMed: 8307887]

26. Keyhani K, Scherer PW, Mozell MM. Numerical Simulation of Airflow in the Human Nasal Cavity. Journal of Biomedical Engineering. 1995;117(4):429–441. doi:10.1115/1.2794204

27. Kurtz DB. Experimental and Numerical Determination of Odorant Solubility in Nasal and Olfactory Mucosa. Chemical Senses. 2004;29(9):763–773. doi:10.1093/chemse/bjh079 [PubMed: 15574812]

28. Scott JW, Sherrill L, Jiang J, Zhao K. Tuning to odor solubility and sorption pattern in olfactory epithelial responses. J Neurosci. 2014 Feb 5;34(6):2025–36. doi: 10.1523/JNEUROSCI.3736-13.2014. [PubMed: 24501345]

29. Smith TD, Rossie JB. Nasal fossa of mouse and dwarf lemurs (primates, cheirogaleidae). Anat Rec (Hoboken). 2008 Aug;291(8):895–915. doi: 10.1002/ar.20724. [PubMed: 18615700]

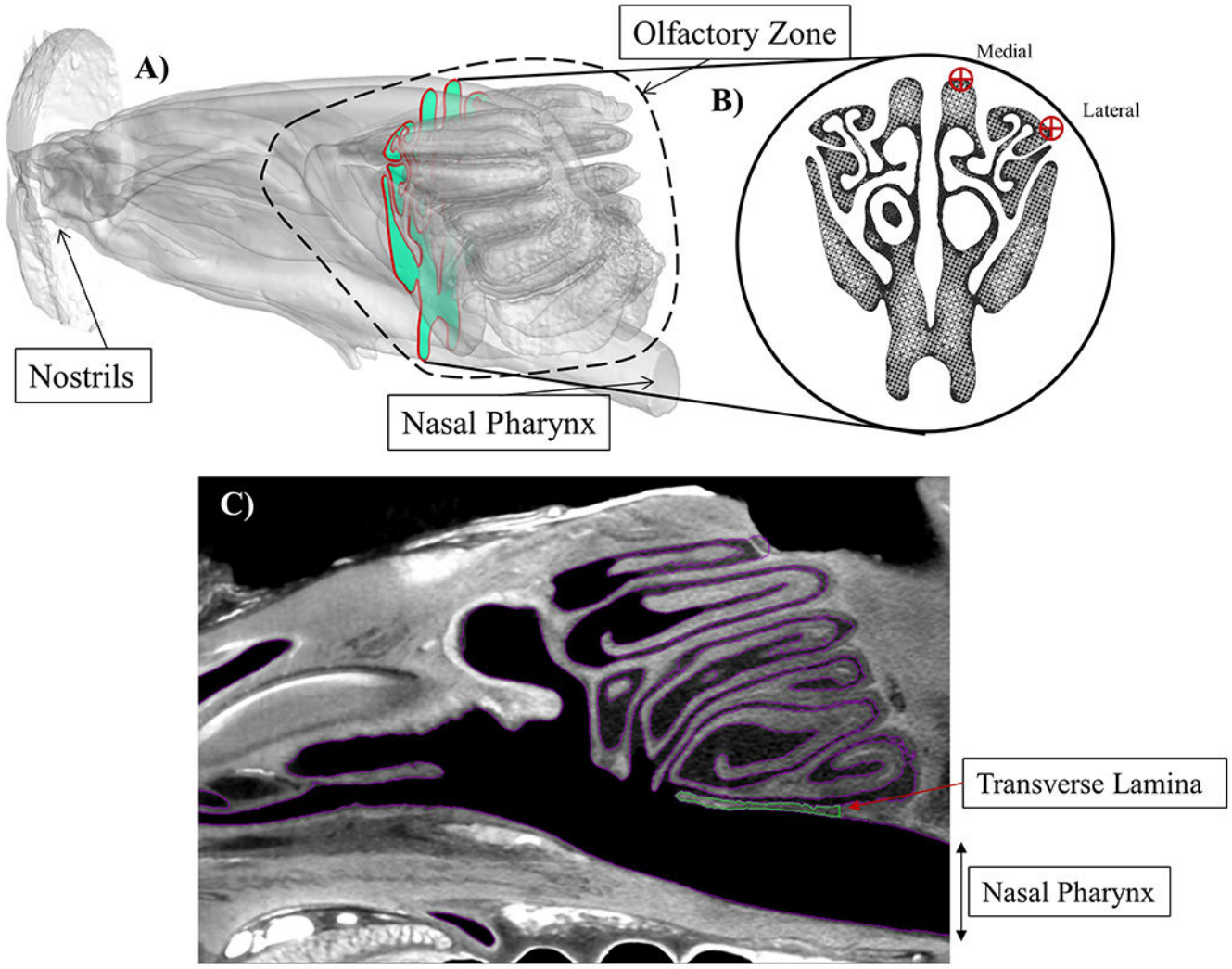

Fig 1.

a) 3D model of rat nasal cavity b) coronal cross section through the olfactory region with the medial and lateral sampling regions highlighted along with internal tetrahedral mesh elements c) sagittal CT cross section of the olfactory region showing the transverse lamina that sequesters airflow from the nasopharynx (highlighted in green)

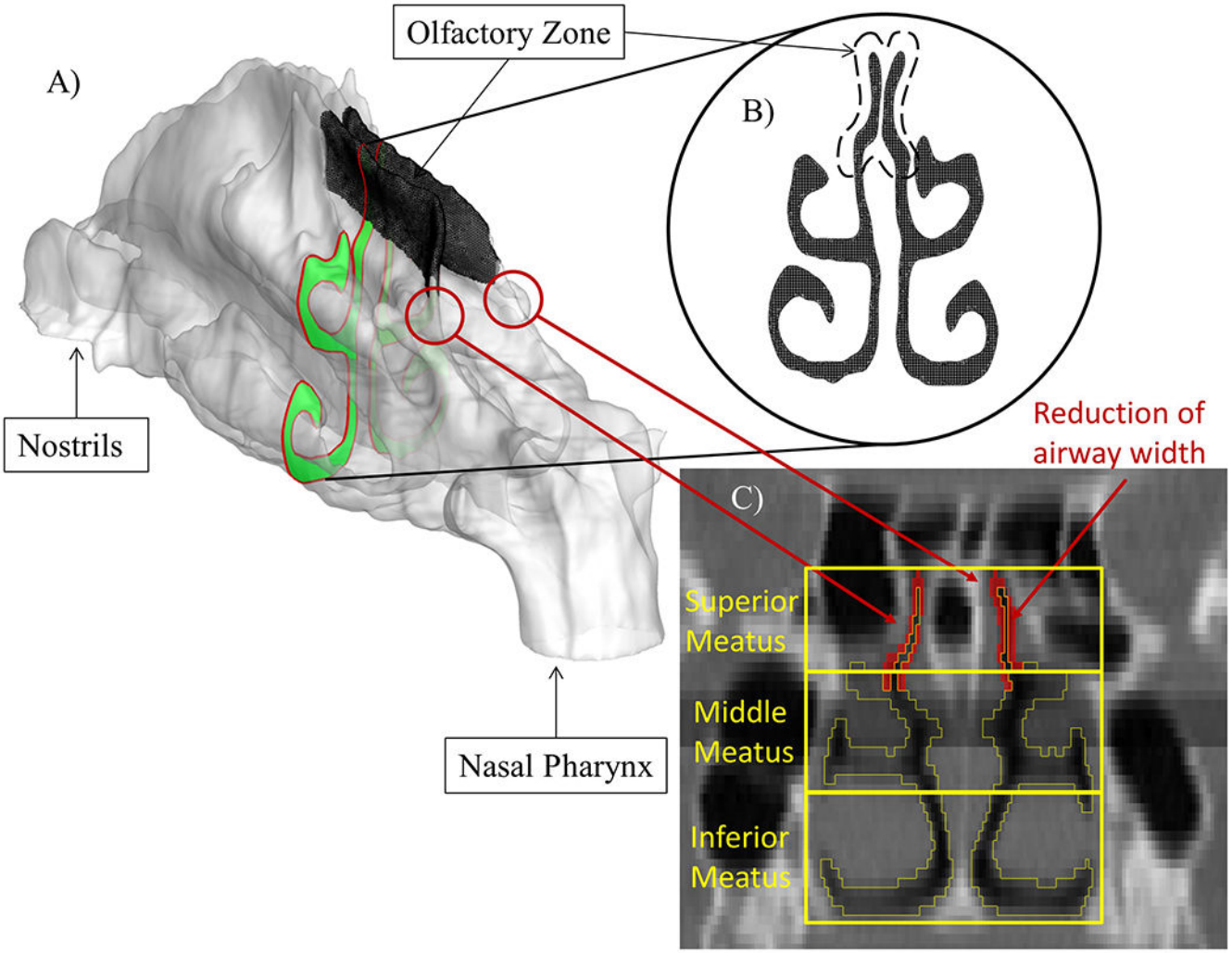

Fig 2.

a) 3D model of human nasal cavity with olfactory region highlighted as surface mesh b) coronal cross section through olfactory region with internal tetrahedral mesh elements c) CT scan image showing reduction in recess that bridges the olfactory region to the nasopharynx with the red highlighted the reduced airway width, along with sections highlighting superior, middle, and inferior meatus.

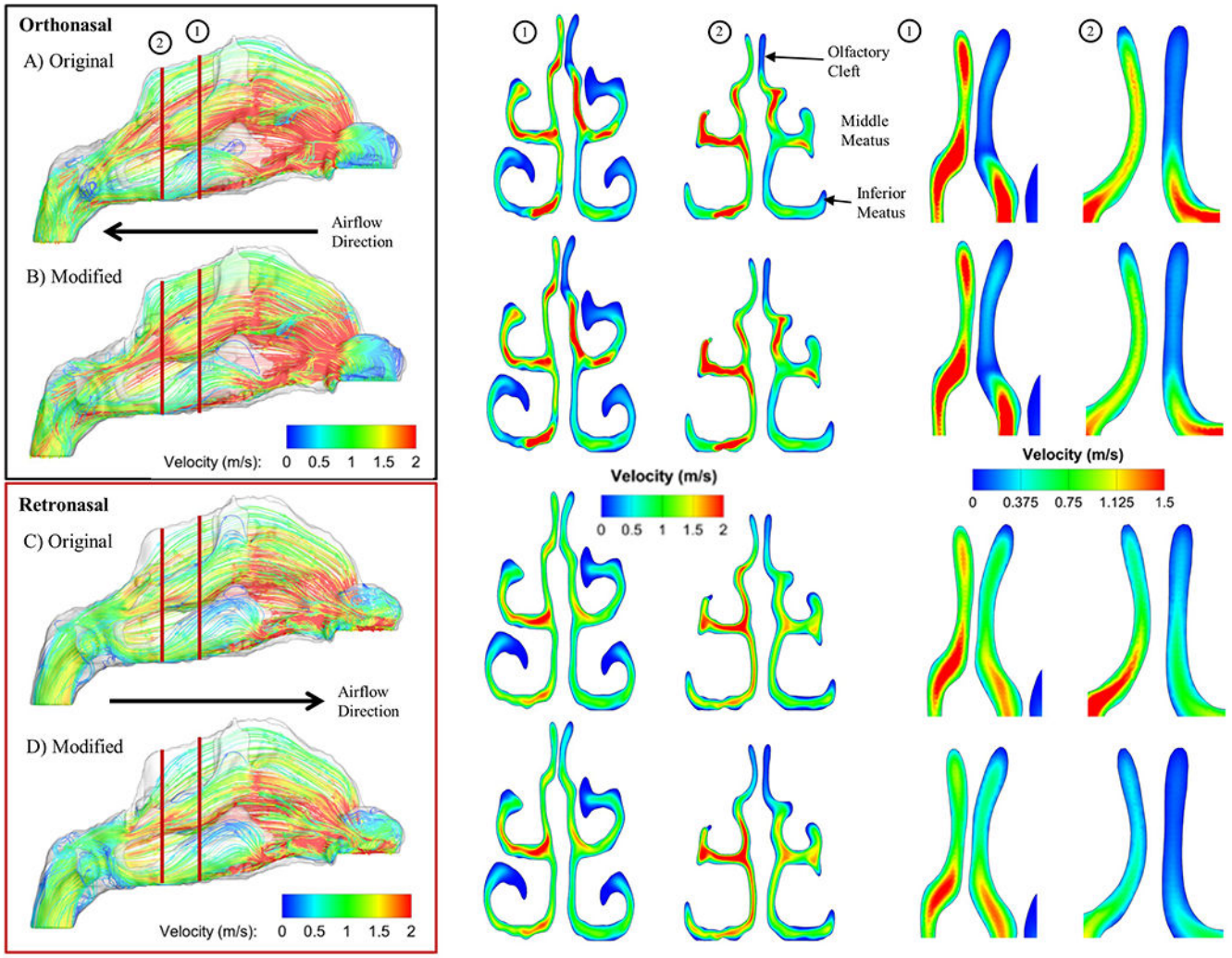

Fig 3.

Velocity streamlines and cross-sectional profiles for human orthonasal and retronasal transport, with (1) and (2) indicating anterior and posterior coronal cross-sections through the olfactory zone, with a magnified cross section view on the right at the region of interest with modified color grading to accentuate contour differences a) original orthonasal transport b) post-modification orthonasal transport c) original retronasal transport d) post-modification retronasal transport

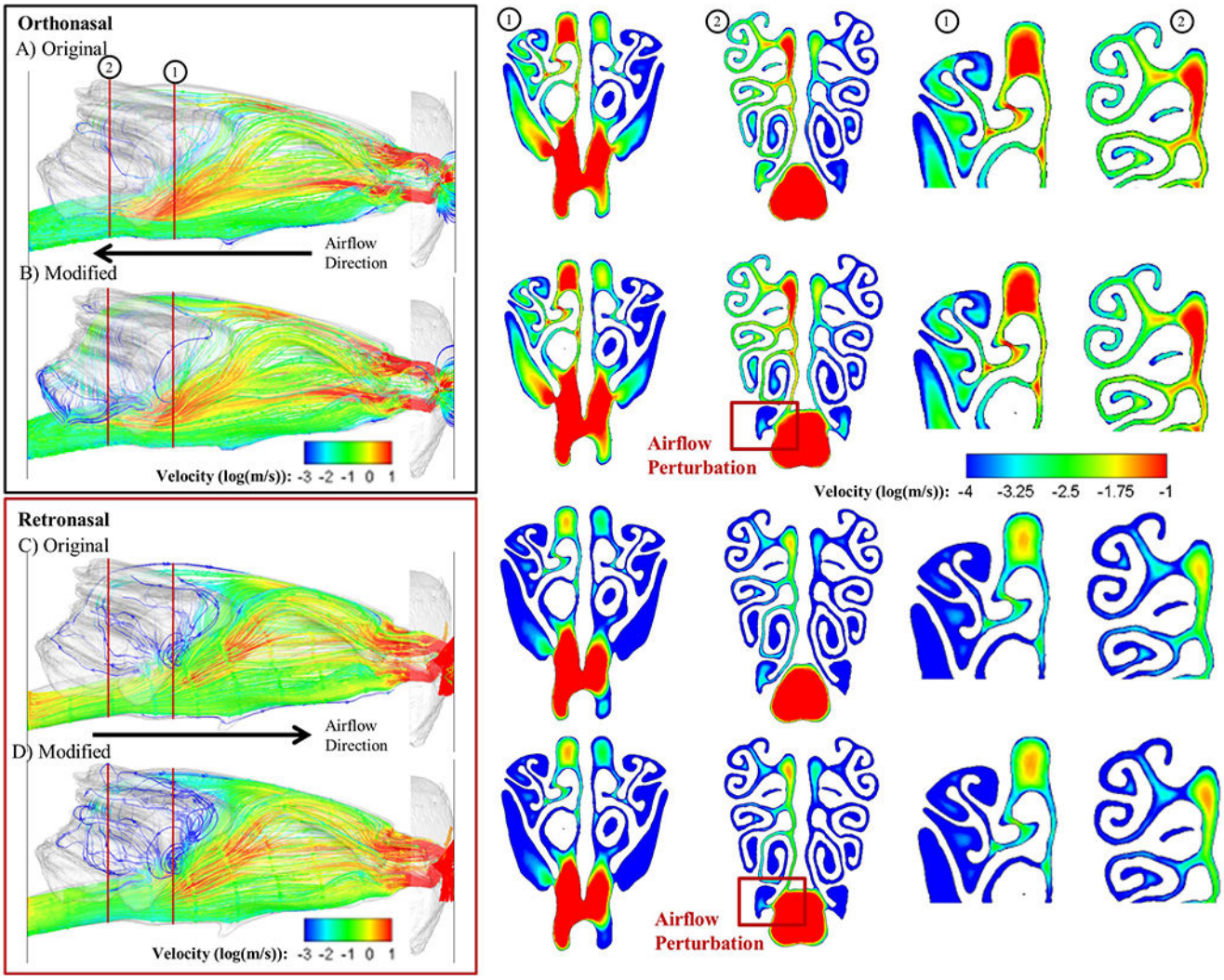

Fig 4.

Velocity streamlines and cross-sectional profiles for rodent orthonasal and retronasal transport, with (1) and (2) indicating anterior and posterior coronal cross-sections through the olfactory zone, with a magnified cross section view on the right at the region of interest with modified color grading to accentuate contour differences a) original orthonasal transport b) post-modification orthonasal transport c) original retronasal transport d) post-modification retronasal transport

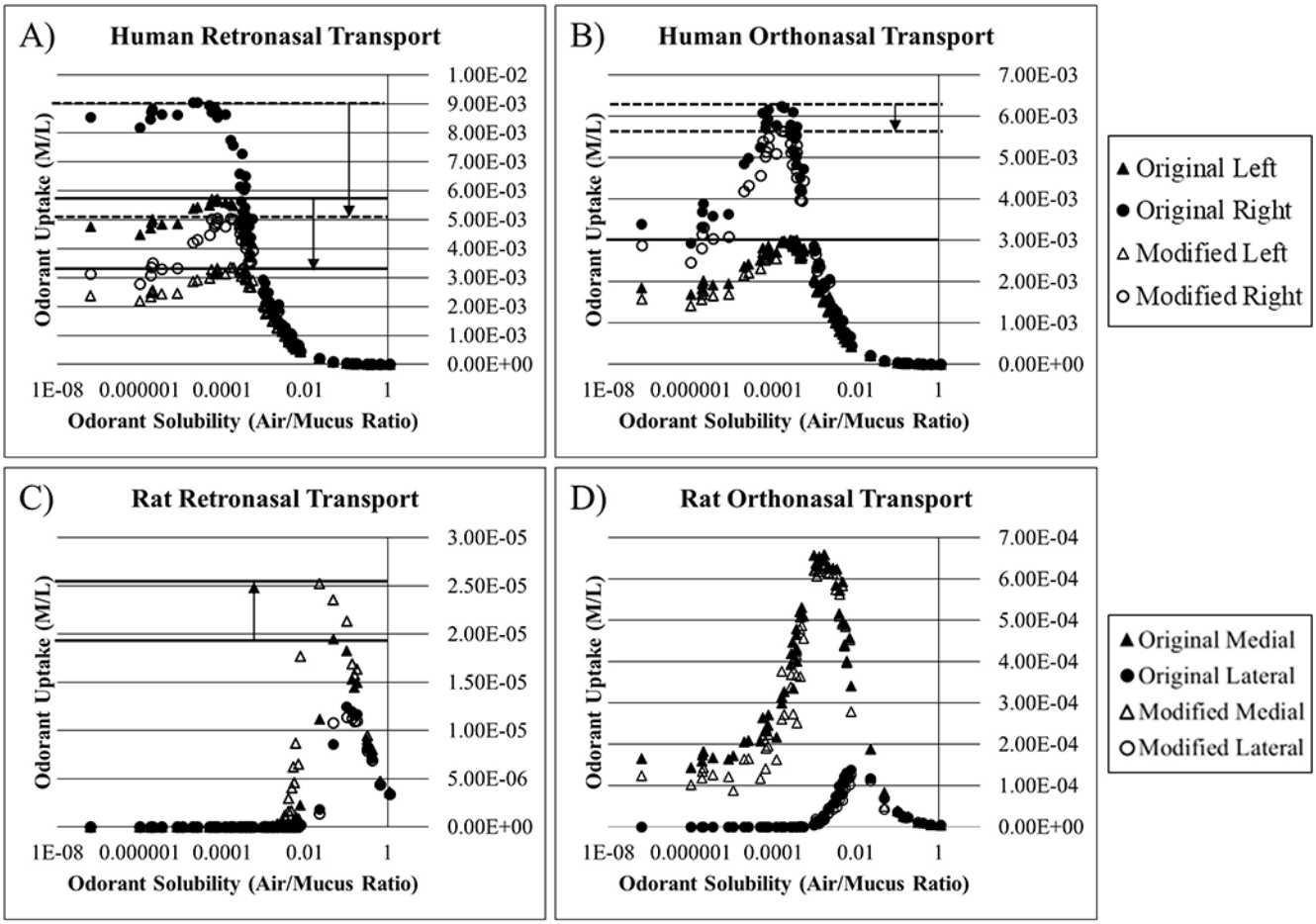

Fig 5.

Comparisons between original and post-modification orthonasal vs retronasal transport in humans and rodents, with the x-axis indicating air/mucus partition coefficient where a smaller value indicates a higher solubility a) human retronasal transport, with dotted line indicating peak odorant uptake for right olfactory zone, and solid line for left olfactory zone with arrow showing direction of change between original and modification b) human orthonasal transport, with dotted line indicating peak odorant uptake for right olfactory zone, and solid line for left olfactory zone with arrow showing direction of change between original and modification c) rat retronasal transport, with dotted line indicating peak odorant uptake for right olfactory zone, and solid line for left olfactory zone with arrow showing direction of change between original and modification d) rat orthonasal transport with dotted line indicating peak odorant uptake for right olfactory zone, and solid line for left olfactory zone with arrow showing direction of change between original and modification

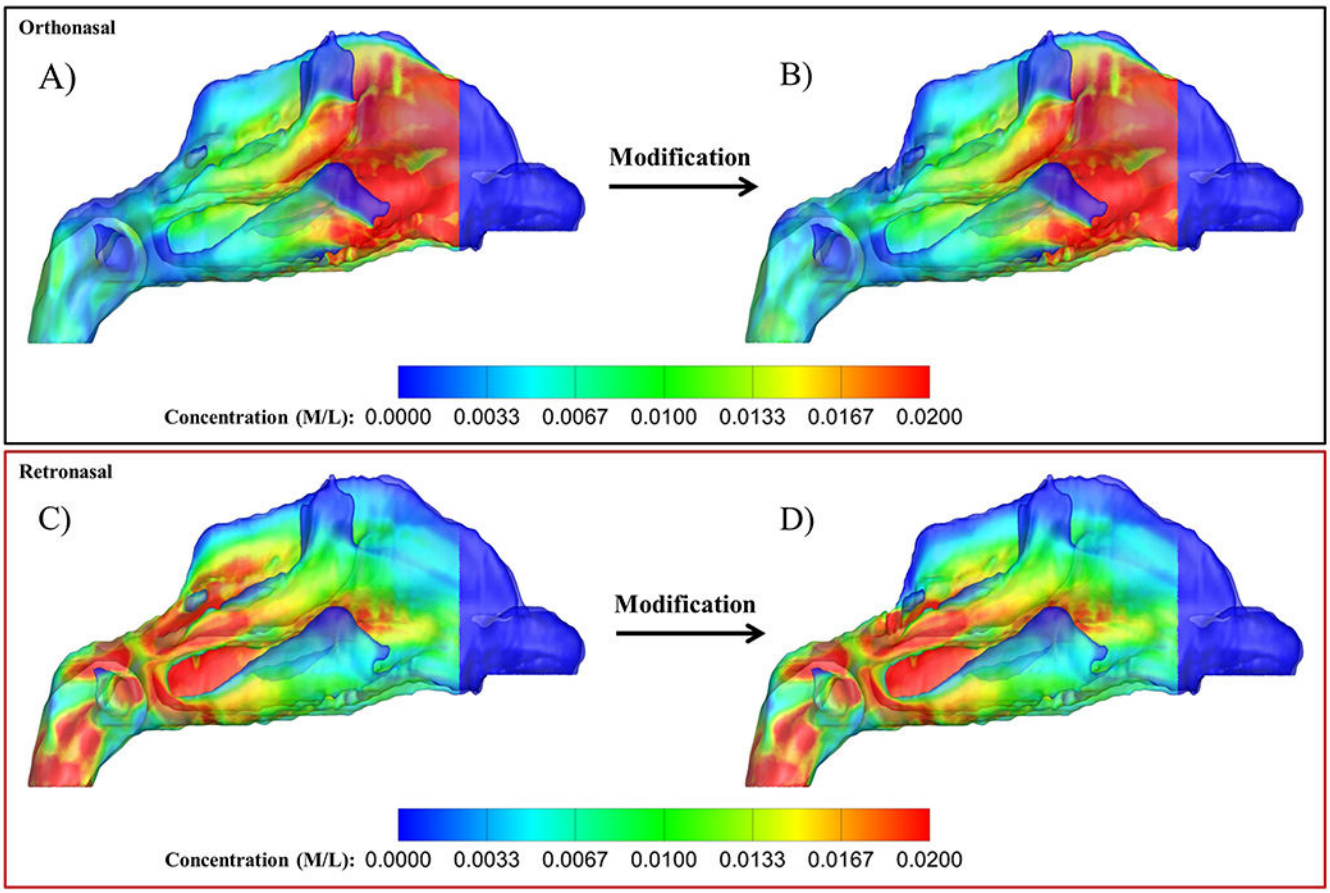

Fig 6.

Odorant absorption distribution map for pyrazine in the human nasal cavity a) original orthonasal transport b) post-modification orthonasal transport c) original retronasal transport d) post-modification retronasal transport

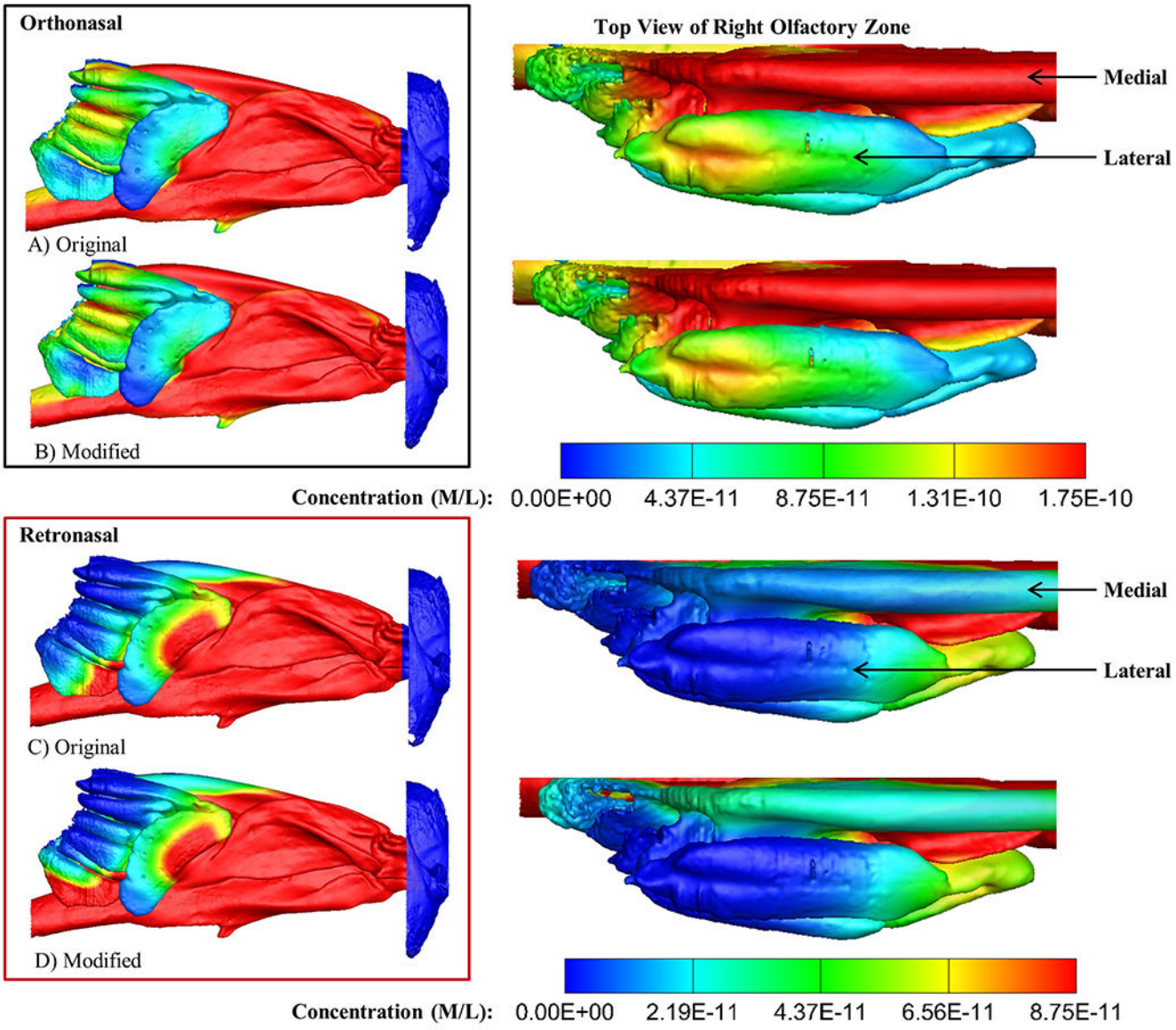

Fig 7.

Odorant absorption distribution map for Toluene in the right rodent nasal cavity and top views a) original orthonasal transport b) post-modification orthonasal transport c) original retronasal transport d) post-modification retronasal transport

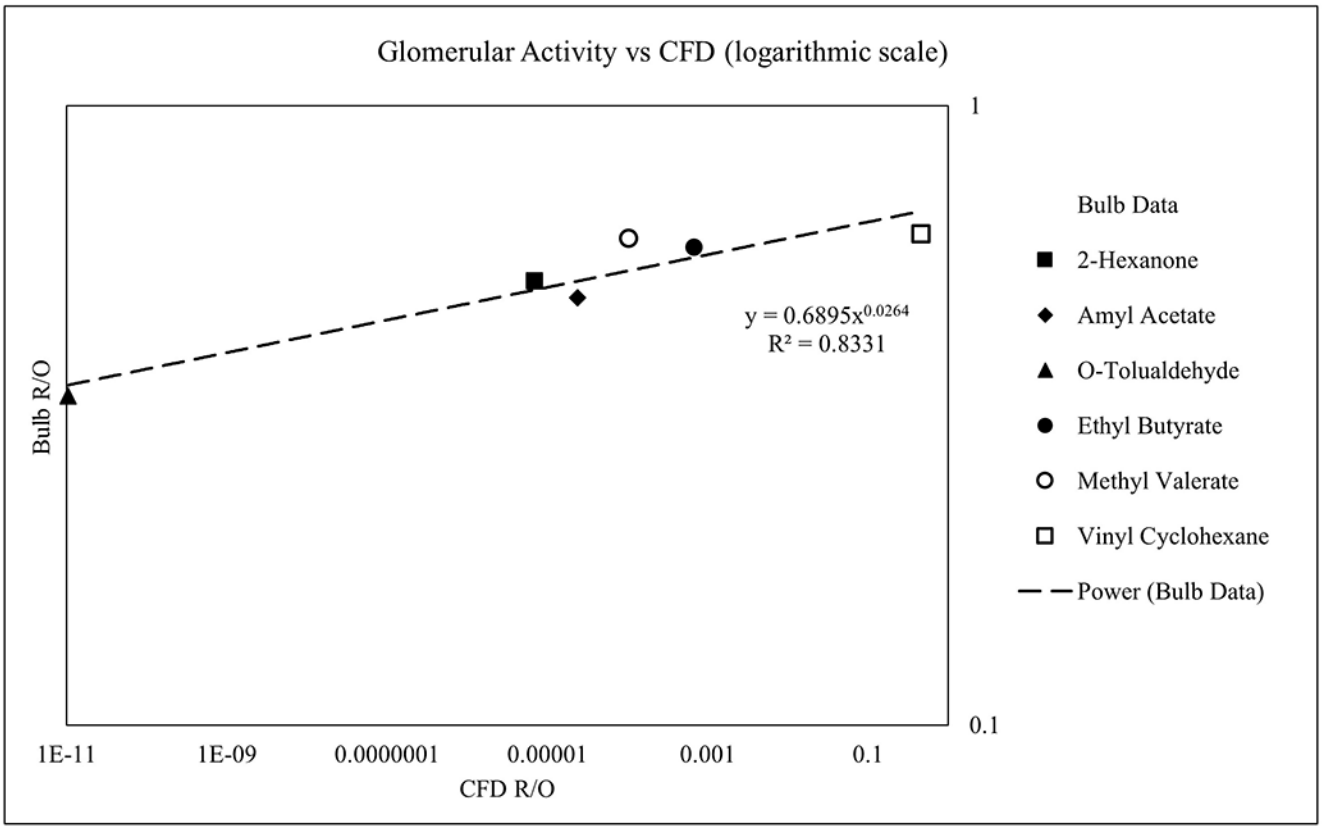

Fig 8.

Correlative relationship between CFD R/O and experimental rat glomerular bulb activity R/O plotted on a logarithmic scale. A Pearson correlation of r=.941, P=.017 was determined between the two variables with a power law curve fit.